

Article

Tuning Metal–Support Interactions on Ni/Al₂O₃ Catalysts to Improve Catalytic Activity and Stability for Dry Reforming of Methane

Lulu He ¹, Yuanhang Ren ¹, Bin Yue ^{1,*}, Shik Chi Edman Tsang ² and Heyong He ^{1,*}

¹ Department of Chemistry and Shanghai Key Laboratory of Molecular Catalysis and Innovative Materials, Fudan University, Shanghai 200438, China; 14110220027@fudan.edu.cn (L.H.); yuanhangren@fudan.edu.cn (Y.R.)

² Wolfson Catalysis Centre, Department of Chemistry, University of Oxford, Oxford OX1 3QR, UK; edman.tsang@chem.ox.ac.uk

* Correspondence: yuebin@fudan.edu.cn (B.Y.); heyonghe@fudan.edu.cn (H.H.); Tel.: +86-21-3124-3916 (H.H.); Fax: +86-21-3124-5572 (H.H.)

Abstract: Ni-based catalysts supported on alumina derived from the pseudo-boehmite prepared by the impregnation method were employed for catalytic dry reforming of methane reaction at the temperature of 550–750 °C. The effect of calcination temperature on physicochemical properties such as the Ni dispersion, reduction degree, nickel crystallite sizes, and metal–support interaction of the catalysts was investigated. The characterization results show that increasing the catalyst calcination temperature leads to the formation of nickel-alumina spinel, which enhances the metal–support interaction and increases the reduction temperature. The nickel nanoparticle size decreases and the effective dispersion increases with the increasing calcination temperature from 450 °C to 750 °C due to the formation of nickel aluminate. The catalyst calcined at 750 °C exhibits the highest CH₄ and CO₂ conversion owing to the small Ni⁰ active sites and high Ni dispersion. In a 200 h stability test in dry reforming of methane at 700 °C, the Ni/Al₂O₃-750 catalyst exhibits excellent catalytic stability and anti-coking ability.

Keywords: carbon dioxide; methane; calcination temperature; dry reforming; nickel particles



Citation: He, L.; Ren, Y.; Yue, B.; Tsang, S.C.E.; He, H. Tuning Metal–Support Interactions on Ni/Al₂O₃ Catalysts to Improve Catalytic Activity and Stability for Dry Reforming of Methane. *Processes* **2021**, *9*, 706. <https://doi.org/10.3390/pr9040706>

Academic Editor: Olivier Monfort

Received: 15 March 2021

Accepted: 14 April 2021

Published: 16 April 2021

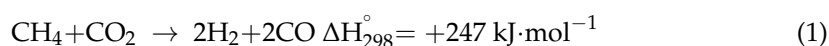
Publisher's Note: MDPI stays neutral with regard to jurisdictional claims in published maps and institutional affiliations.



Copyright: © 2021 by the authors. Licensee MDPI, Basel, Switzerland. This article is an open access article distributed under the terms and conditions of the Creative Commons Attribution (CC BY) license (<https://creativecommons.org/licenses/by/4.0/>).

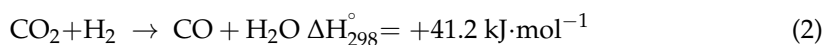
1. Introduction

With the huge development of modern industrialization, global warming and climate change caused by CO₂ emission from the combustion of conventional fossil fuels have become serious problems in recent years [1,2]. Meanwhile, CH₄ from petroleum resources and landfills is also a major contributor to greenhouse gases [3,4]. As an abundant alternative to petroleum and coal, natural gas and biogas that are rich in CH₄ have become the main energy resources [5–8]. Therefore, the dry reforming of methane (Equation (1)), which can simultaneously utilize methane and carbon dioxide, is significant to alleviate the energy crisis and to reduce greenhouse gas emissions [9–11]. Compared with the partial oxidation and steam reforming of methane, dry reforming of methane is industrially advantageous due to the syngas with a low H₂/CO molar ratio of nearly 1, which is more appropriate for the synthesis of hydrocarbons with long-chain through the Fischer–Tropsch reaction [12–15].



The stable structure of CH₄ and CO₂, owing to their high bond energies, makes the dry reforming of methane a very challenging task [16–18]. Furthermore, the endothermic dry reforming of methane reaction is always performed at high temperatures. The reverse

water gas shift reaction (RWGS; Equation (2)), which occurred as a side reaction, causes higher CO₂ conversion than that of CH₄ and the H₂/CO ratio lower than 1 [19,20].



Over the past decades, many kinds of metal catalysts have been widely investigated for the dry reforming of methane reaction. Noble metals, such as Ru, Rh, Pt, Ir, and Pd, exhibit excellent catalytic performance and coke resistance [21–25]. However, they are not suitable for scaled-up industrial applications because of their high cost and scarcity. As an economic substitute, Ni-based catalysts have been studied extensively due to the low cost and comparable catalytic activity to noble metals [11,26]. A big drawback of Ni-based catalysts is that they are always suffering from rapid deactivation because of coking deposition and sintering of Ni nanoparticles [20,27,28]. In the dry reforming of methane reaction, coke formation is mainly caused by the methane decomposition reaction (Equation (3)) and the CO disproportionation reaction (Equation (4)):



Therefore, preventing the sintering of Ni active sites and reducing the amount of carbon deposition on Ni-based catalysts are of great significance from both the academic and industrial perspectives. Great efforts have been focused on improving catalytic performance and catalyst stability by loading Ni on various oxide supports, such as CeO₂, SiO₂, ZrO₂, Al₂O₃, MgO, etc. [29–33]. The supports were shown to play an important role in catalytic performance and coke formation. The interaction between active metal component and support influences the structure of catalysts, the particle size, and the dispersion of active sites, affecting the catalytic performance and stability of catalysts. Furthermore, catalysts with high metal dispersion and small metal nanoparticles caused by strong metal–support interaction have been proved to exhibit excellent catalytic performance [31].

Ni supported on alumina is a promising catalyst for large-scale industrial application because of its affordability and thermal stability. The alumina surface (the γ form) has certain acidity and functional groups like hydroxyl that could enhance metal–support interaction [27,31,34,35]. Kumar et al. studied the catalytic performance of Ni-based catalysts with diverse support materials (Al₂O₃, TiO₂, ZrO₂, SBA-15, MgO, and CeO₂-ZrO₂) for the methane reforming reactions. The Al₂O₃-supported Ni catalyst had the best catalytic performance in the reaction conditions studied, which could be attributed to the well-dispersed small Ni nanoparticles, strong metal–support interaction, high reduction degree, and high basic site concentration in the Ni/Al₂O₃ catalyst [36]. Our previous work also found that Ni/Al₂O₃ spinel-derived catalysts possessed a large number of well-dispersed, small Ni⁰ particles which could yield outstanding activity and stability under optimized reaction conditions [34]. Several studies investigated the effect of calcination temperature on the supported active metal species [32,37–41]. Calcination temperature has a great influence on the dispersion of active metal particles and the metal–support interaction, thus affecting the activity and stability of catalysts. Zhang et al. investigated the relationship between the interaction of Ni species and alumina versus calcination temperature during the steam reforming of acetic acid. They found that high calcination temperature resulted in the formation of nickel-alumina spinel, which strengthened the interaction between nickel species with alumina. After the nickel-alumina spinel was completely reduced, the catalyst exhibited good activity [42]. Wang et al. revealed that calcination temperature significantly affected the Ni particle size, the degree of reduction, metal–support interaction, and surface Ni active species content. Calcination temperature is pivotal to determine the activity and stability of the Ni-based catalysts in steam reforming ethanol reaction [43].

The study of the relationships between the metal–support interaction of Ni-based catalysts and calcination temperature is expected to have a crucial impact in enhancing

the catalytic performance in dry reforming of methane reaction. In the present work, we investigate the effect of calcination temperature on the catalytic performance of alumina supported Ni-based catalysts in dry reforming of methane reaction. A series of Ni-based catalysts supported on alumina derived from the pseudo-boehmite were prepared by the simple wet impregnation method, and then calcined at different temperatures (450, 550, 650, and 750 °C). The effects of calcination temperature on Ni dispersion, metal nanoparticle size, and reduction degree were investigated by various techniques. The characterization results of the catalysts calcined at different temperatures are correlated to their activity and stability in the dry reforming of methane reaction.

2. Materials and Methods

2.1. Catalyst Preparation

The alumina support was derived from the calcination of pseudo-boehmite precursor (Shandong City Star Petroleum Chemical Technology Co. Ltd., Shandong, China) at 750 °C for 3 h. The catalysts were prepared through the wet impregnation method; 0.49 g of $\text{Ni}(\text{NO}_3)_2 \cdot 6\text{H}_2\text{O}$ was initially dissolved in 16 mL of water and 1.0 g of support power was then added into the nickel nitrate solution. The mixture was magnetically stirred overnight at room temperature, and the excess water was removed from the slurry in a rotary evaporator operating at 60 °C. The solids were dried at 120 °C for 12 h and calcined at different temperatures (450, 550, 650, and 750 °C) for 3 h at a heating rate of 1 °C·min⁻¹ from room temperature in a muffle furnace. The as-prepared samples were denoted as Ni/Al₂O₃-x (x represented the calcination temperature), and the loading of metal Ni was 10 wt.%.

2.2. Catalyst Characterization

The nickel content of the calcined catalysts was decided by inductively coupled plasma atomic emission spectrometer (ICP-AES) performed on a Thermo Elemental IRIS Intrepid apparatus. Before the analysis, 10 mg catalyst power was digested at 100 °C for 3 h in a mixed acid solution of 2 mL concentrated nitric acid (67 wt.%) and 3 mL hydrochloric acid (37 wt.%).

Transmission electron microscopy (TEM) was obtained on a JEOL JEM2011 electron microscope. The catalysts were ultrasonically suspended in anhydrous ethanol. The suspension was then dropped onto a copper grid-supported transparent carbon foil and dried in the air.

The specific surface area, pore volume, and average pore size of different samples were measured from the N₂ adsorption–desorption isotherms at –196 °C using a Micromeritics Tristar 3000 apparatus. Before the measurements, the sample was degassed under vacuum at 250 °C for 3 h. The Brunauer–Emmett–Teller (BET) method was applied to calculate the specific surface areas of the catalysts. The cumulative volumes of pores and average pore diameters were calculated from the desorption branch of the nitrogen isotherms by the Barrett–Joyner–Halenda (BJH) model.

X-ray diffraction (XRD; Bruker D8 Advance diffractometer) with Cu K α radiation ($\lambda = 1.5418 \text{ \AA}$) was used to characterize the samples at 40 kV and 40 mA. The samples were scanned in the range of 10° to 80°, a step size of 0.01°, and a step time of 0.6 s. The average crystallite size of the metallic Ni was estimated according to the Scherrer equation.

The surface composition of the catalysts was analyzed by X-ray photoelectron spectroscopy (XPS; Versa Probe PHI 5000, Al K α). The binding energies were calibrated using the containment carbon (C1s = 284.6 eV).

The reducibility of the catalysts was studied by H₂ temperature-programmed reduction (H₂-TPR) using a Micromeritics ChemiSorb 2720 apparatus with a thermal conductivity detector (TCD). Before measurement, ~45.0 mg catalyst was placed in a U-shape quartz tube and degassed under Ar at 200 °C for 2 h to remove the adsorbed moisture and impurities. The sample was cooled to room temperature and the was gas changed to 10% H₂/Ar.

Then, the sample was reduced in a stream of 10% H₂/Ar (50 mL·min⁻¹) with a heating rate of 10 °C·min⁻¹ from room temperature up to 900 °C.

H₂ temperature-programmed desorption (H₂-TPD) experiments were also carried out on a Micromeritics ChemiSorb 2720 apparatus. Approximately 100 mg of catalyst was placed into the quartz tube and reduced with a flow of 10% H₂/Ar (50 mL min⁻¹) at 750 °C for 90 min. After reduction, the sample was cooled down to 40 °C and then purged with Ar flow (50 mL min⁻¹) for 1 h to remove weakly adsorbed species on the surface. The desorption process was carried out by increasing the temperature of the sample from 40 to 700 °C at a heating rate of 10 °C min⁻¹ under the flow of Ar. The amount of desorbed H₂ was calculated by integrating the area of the H₂-TPD profiles, and the equipment was prior calibrated using Ag₂O reduction as the reference. The Ni dispersion was calculated based on the stoichiometry of H:Ni_{surface} = 1:1.

The amount of deposited carbon in the stability test was evaluated by the thermogravimetric analysis performed on SDT Q600 integrated thermal analyzer. The spent catalyst (~5 mg) was heated under the flow of air (100 mL min⁻¹) from room temperature to 900 °C with a heating rate of 10 °C min⁻¹.

2.3. Catalytic Activity and Stability Tests

A fixed-bed reactor system was used to test the catalytic activity and stability tests for dry reforming of methane using a quartz tube with an inner diameter of 5 mm and a length of 48 cm at atmospheric pressure. The gas flow rate was controlled by mass-flow controllers. Typically, 30 mg catalyst (40–60 mesh) was mixed with 250 mg inert quartz sand (40–60 mesh) and placed into the reactor. The catalyst was reduced in a flow of H₂ (30 mL·min⁻¹) at 750 °C for 90 min before the reaction, then purged with Ar for 40 min. Then, the reaction gas (CO₂:CH₄:Ar volume ratio of 1:1:3) was introduced with a gas hourly space velocity (GHSV) of 24,000 mL h⁻¹ g⁻¹. The effluent product gases were cooled in an ice-water bath and analyzed by online gas chromatography with a thermal conductivity detector (TCD) using a TDX-01 packed column. The catalytic activity of the catalysts was tested at the temperature range of 550 to 750 °C. A long-term stability test was performed at 700 °C for 50 and 200 h under identical conditions. The conversions of CH₄ and CO₂ were calculated using the following formulae:

$$\text{Conversion of CH}_4 (\%) = \frac{F_{\text{CH}_4,\text{in}} - F_{\text{CH}_4,\text{out}}}{F_{\text{CH}_4,\text{in}}} \times 100\%$$

$$\text{Conversion of CO}_2 (\%) = \frac{F_{\text{CO}_2,\text{in}} - F_{\text{CO}_2,\text{out}}}{F_{\text{CO}_2,\text{in}}} \times 100\%$$

where $F_{\text{CH}_4,\text{in}}$ and $F_{\text{CO}_2,\text{in}}$ represent the inlet flow rates of CH₄ and CO₂, respectively, and $F_{\text{CH}_4,\text{out}}$ and $F_{\text{CO}_2,\text{out}}$ represent the outlet flow rates of outlet CH₄ and CO₂, respectively.

3. Results and Discussion

3.1. Effect of Calcination Temperature on the Physicochemical Properties of Ni/Al₂O₃ Samples

3.1.1. ICP-AES and N₂ Adsorption-Desorption Analysis

The chemical compositions of the calcined Ni/Al₂O_{3-x} samples are summarized in Table 1. ICP-AES was performed to determine the exact Ni content of the calcined samples, and the results show that the measured Ni contents are consistent with the theoretical values. The influence of calcination temperature on physicochemical properties of the samples was investigated by the N₂ adsorption-desorption analysis, and the results are presented in Figure 1. The alumina support and calcined samples exhibit type IV isotherms coupled with the hysteresis loop [34,43]. This indicates that alumina support and Ni/Al₂O₃ catalysts calcined at different temperatures have a typical mesoporous structure. The corresponding surface area, pore volume, and average pore diameter are also presented in Table 1. The surface area, pore volume, and average pore diameter of Al₂O₃ support are 214 m² g⁻¹, 1.14 cm³ g⁻¹, and 10.2 nm, respectively. After Ni impregnation into

Al₂O₃ support, the surface area and pore volume of Ni/Al₂O₃ samples decrease with the increasing calcination temperature. It is also found that the hysteresis loop shifts slightly toward the high relative pressure with increase of calcination temperature as shown in Figure 1. It has been generally accepted that the shift of the hysteresis loop toward to high relative pressures indicates the existence of larger pore diameters [37], which is consistent with the average pore diameter result in Table 1.

Table 1. Physicochemical properties of the Al₂O₃ support and the calcined Ni/Al₂O₃-x samples.

Samples	Ni Content (wt.%) ¹	BET Surface Area (m ² g ⁻¹)	Pore Volume (cm ³ g ⁻¹)	Average Pore Diameter (nm)
Al ₂ O ₃	-	214	1.14	10.2
Ni/Al ₂ O ₃ -450	9.6	201	1.06	10.4
Ni/Al ₂ O ₃ -550	9.9	192	0.89	11.0
Ni/Al ₂ O ₃ -650	10.0	173	0.74	11.8
Ni/Al ₂ O ₃ -750	9.6	165	0.67	12.9

¹ Analyzed by ICP-AES.

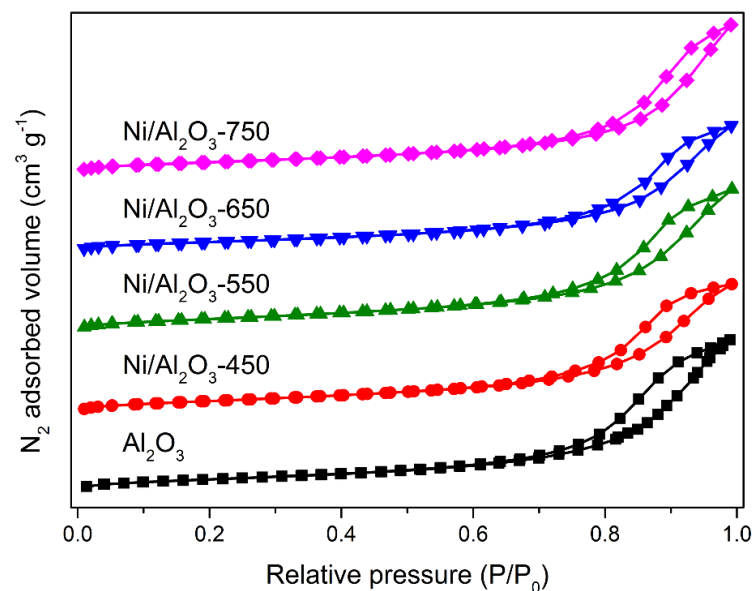


Figure 1. N₂ adsorption–desorption isotherms of Al₂O₃ support and Ni/Al₂O₃ samples calcined at different temperatures.

3.1.2. XRD Characterization

Figure 2 shows the XRD patterns of the Al₂O₃ support and Ni/Al₂O₃ samples treated at different calcination temperatures. All the samples exhibit the diffraction peaks at 2θ of 37.6°, 39.5°, 45.9°, and 67.0°, which correspond to the (311), (222), (400), and (440) diffractions of γ-Al₂O₃ (PDF No. 10-0425), respectively [43,44]. For the Ni/Al₂O₃-450 and Ni/Al₂O₃-550 samples, there is a weak peak at 2θ of 43.3° assigned to the (200) diffractions of NiO (PDF No. 04-0835) without observable peaks assigned to the NiAl₂O₄ phase, indicating the NiO phase may be the main component in Ni/Al₂O₃-450 and Ni/Al₂O₃-550 [25,40]. With increasing calcination temperature, the diffractions of the NiO phase disappear gradually, and instead three new peaks at 2θ of 19.1°, 31.6°, and 59.7°, corresponding to the (111), (220), and (511) diffractions of NiAl₂O₄ spinel (PDF No. 10-0339), are observed in the Ni/Al₂O₃-650 and Ni/Al₂O₃-750 samples [34,44]. Moreover, the intensity of NiAl₂O₄ spinel phase in Ni/Al₂O₃-750 is much stronger than that in Ni/Al₂O₃-650, indicating more NiAl₂O₄ spinel phase exists at high calcination temperature. In the catalysts calcined at different temperatures, the Ni species assigned to NiO or NiAl₂O₄ cannot be distinguished by XRD results because of the overlapped diffraction peaks of NiO, Al₂O₃, and NiAl₂O₄.

Therefore, the effect of calcination temperature on the Ni species of Ni/Al₂O₃ samples will be further investigated with H₂-TPR and XPS analysis below.

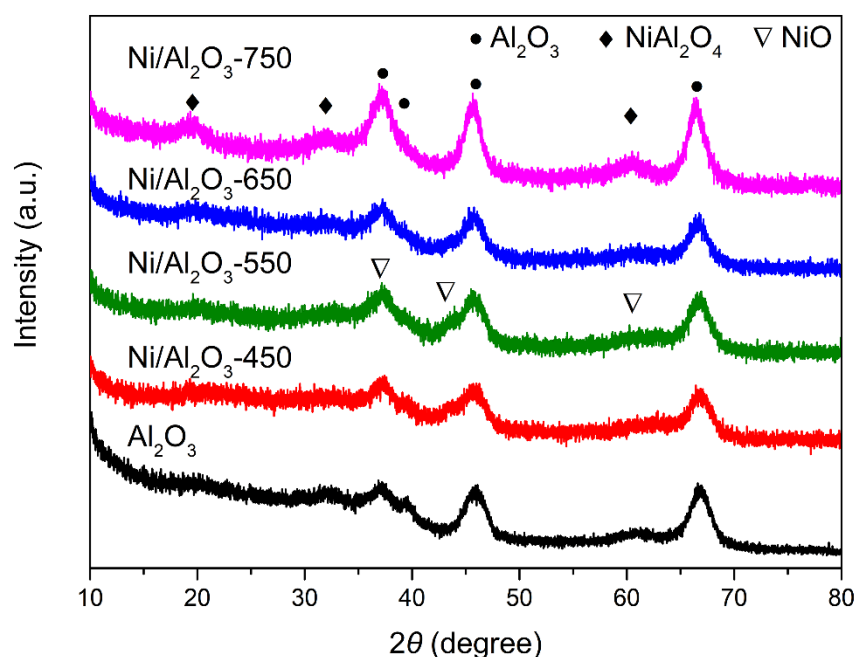


Figure 2. XRD patterns of the Al₂O₃ support and Ni/Al₂O₃ samples calcined at different temperatures.

XRD patterns of the reduced catalysts are shown in Figure 3. The diffractions of γ -Al₂O₃ are observed for all samples, indicating that the structure of Al₂O₃ support maintains after reduction. Three new peaks at 2θ of 44.5°, 51.9°, and 76.4° are observed for all the catalysts after reduction in H₂, which can be assigned to the (111), (200), and (220) lattice planes of metallic Ni (PDF No. 04-0850), respectively [33,45]. The XRD results show that the intensity of the metallic Ni phase decreases with increasing calcination temperature. The amount of Ni⁰ species decreases with increasing calcination temperature, indicating the metal–support interaction between Ni species and the alumina support is stronger and the Ni species are more difficult to reduce at the higher temperature. The Ni nanoparticle size was estimated from Ni (200) diffraction peak using the Scherrer equation, and the results are given in Table 2. The particle size of the Ni⁰ decreases with the increasing calcination temperature. The high calcination temperature facilitates the nickel oxides to react with the alumina support and strengthens the metal–support interaction through the formation of the NiAl₂O₄ spinel phase. Therefore, Ni species can be reduced to form small Ni particles.

Table 2. Crystallite size, reduction degree, and dispersion of Ni/Al₂O₃-x catalysts after reduction with H₂ at 750 °C for 90 min.

Samples	Ni Particle Size (nm) ¹	Degree of Reduction (%) ²	Dispersion (%) ³	Effective Dispersion (%) ⁴
Ni/Al ₂ O ₃ -450	12.6	91.6	4.3	4.7
Ni/Al ₂ O ₃ -550	11.5	87.4	4.5	5.1
Ni/Al ₂ O ₃ -650	10.2	80.9	4.6	5.7
Ni/Al ₂ O ₃ -750	9.2	71.6	5.2	7.3

¹ Estimated from Ni (200) ($2\theta = 51.9^\circ$) diffraction peak using Scherrer equation. ² Calculated based on the H₂ consumption during the reduction processes. ³ Calculated based on the H₂ desorption amount during H₂-TPD. ⁴ Effective dispersion = dispersion/degree of reduction \times 100%.

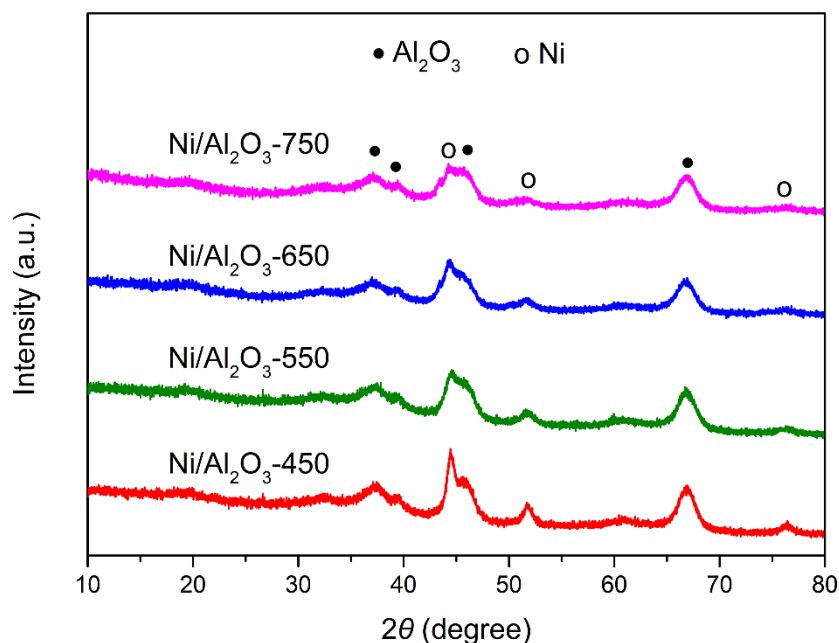


Figure 3. XRD patterns of Ni/Al₂O_{3-x} catalysts reduced in H₂ at 750 °C for 90 min.

3.1.3. TEM Analysis

The morphology of the samples calcined at different temperatures has been characterized by TEM. As it can be seen in Figure 4, all samples present similar morphology at the nanoscale and do not change significantly with increasing calcination temperature. Combining with the XRD results that all catalysts exhibit the diffraction peaks correspond to γ -Al₂O₃ phase, it can be proved that the Ni/Al₂O_{3-x} samples possess favorable thermal stability after being calcined up to 750 °C in this work. The TEM images and Ni particle size distributions of the reduced catalysts are shown in Figure S1. The average Ni nanoparticle sizes of the reduced catalysts are 12.4 nm, 11.8 nm, 10.3 nm, and 9.5 nm for Ni/Al₂O₃-450, Ni/Al₂O₃-550, Ni/Al₂O₃-650, and Ni/Al₂O₃-750, respectively. The results are in agreement with the XRD results in Table 2.

3.1.4. H₂-TPR and H₂-TPD Analysis

H₂-TPR was performed to study the nickel reducibility and the metal–support interactions to identify the nature of Ni species. As showed in Figure 5, the reducible NiO species shown in the H₂-TPR study are usually classified into three types: (1) the peak located in the low-temperature region of 300 to 550 °C is typically assigned to the α -type NiO species that have weak interaction with the alumina support, (2) the moderate-temperature peak in the range of 550 to 700 °C represents the β -type NiO species with the strong interaction with alumina, and (3) the reduction peak located in the high-temperature region of more than 700 °C is assigned to the γ -type NiO species which is attributed to the stable nickel aluminate phase with a spinel structure [40,43,44,46]. From the H₂-TPR results, the α -type and β -type NiO species mainly exist in Ni/Al₂O₃-450, with a small shoulder at ~720 °C corresponding to the NiAl₂O₄ species which can be detected in the XRD pattern. The reduction peaks of the α -type and β -type NiO species shift to high temperature for Ni/Al₂O₃-550 and Ni/Al₂O₃-650, and no obvious peak assigned to the α -type NiO species appears in Ni/Al₂O₃-750. Meanwhile, the peaks assigned to the NiAl₂O₄ phase (γ -type species) increase their intensity and shift to high temperature with the increase of calcination temperature. These results also clearly show that NiO species and Al₂O₃ can react to form NiAl₂O₄ at high temperature, which is in agreement with the XRD study (Figure 2). Based on the results of H₂-TPR, the reduction degree of Ni was obtained (Table 2). The reduction degree of catalysts shows a trend of decrease with the increasing calcination temperature,

indicating that the calcination temperature promotes the interaction between nickel species and alumina support, which makes the reduction of Ni^{2+} species with H_2 difficult [32,43].

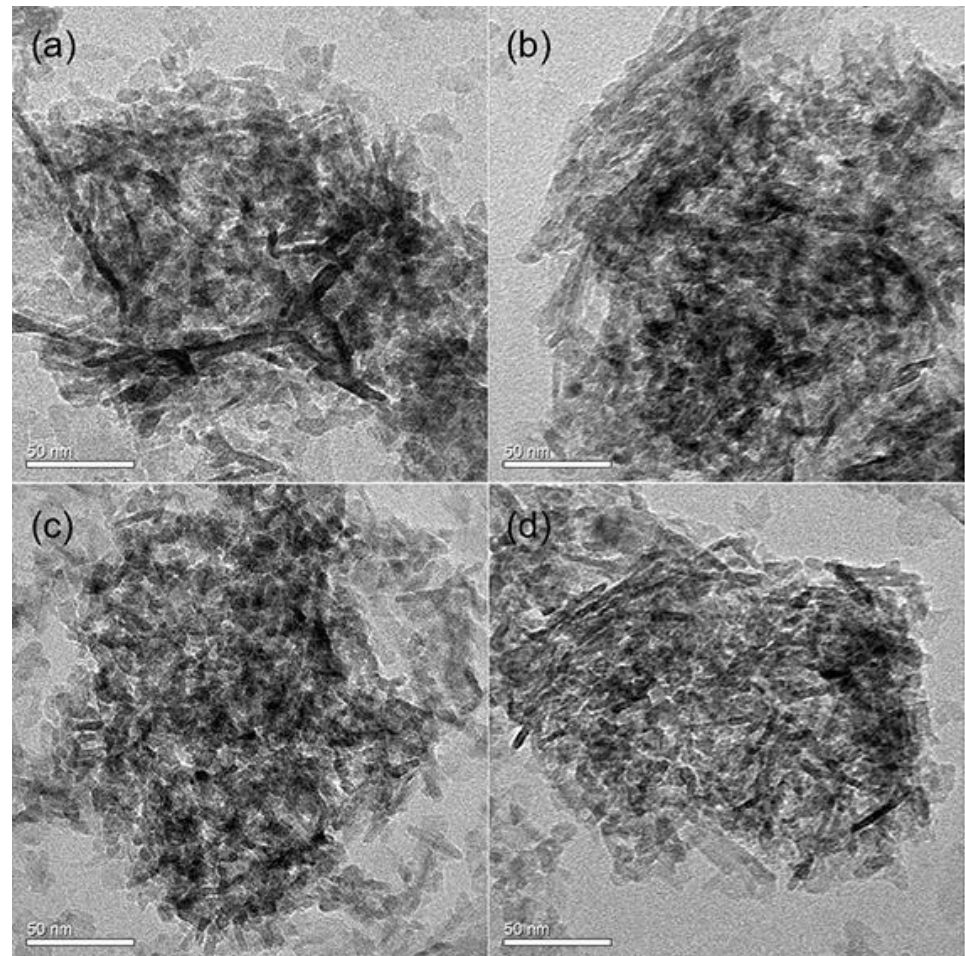


Figure 4. TEM images of the samples calcined at different temperatures: (a) Ni/Al₂O₃-450, (b) Ni/Al₂O₃-550, (c) Ni/Al₂O₃-650, and (d) Ni/Al₂O₃-750.

The metal dispersion was measured by H_2 -TPD, and the effective Ni dispersion calculated are given in Table 2. The results show that the nickel crystallite sizes decrease with the increase of calcination temperature, which can be attributed to the strong metal–support interaction at high temperature. Although the reduction degree decreases with the increase in calcination temperature, the effective dispersions of Ni increase. During the formation of NiAl_2O_4 species at high calcination temperature, the reaction of surface nickel oxide with alumina support not only prevents the migration of nickel particles over the surface leading to sintering, but also stabilizes the high dispersion of nickel on the support resulting in high dispersion of Ni species. [25,47,48].

3.1.5. X-ray Photoelectron Spectroscopy Analysis

XPS analysis was carried out to further confirm the chemical state of nickel in the calcined Ni/Al₂O₃ catalysts. Figure 6 shows Ni 2p_{3/2} signals of the samples calcined at different temperatures. The deconvolution of the main XPS peak in the Ni 2p_{3/2} region displays two peaks, indicating that there are two kinds of Ni species in the catalysts. The peak located at 854.6 eV is associated with NiO species exhibiting interaction with Al₂O₃ support, and the peak observed at 856.5 eV is assigned to the Ni^{2+} ions in the NiAl_2O_4 the spinel phase of which is harder to reduce than NiO species [46,49–51]. In Ni/Al₂O₃-450, the spectrum clearly shows that the main Ni species is NiO. The content

of NiO species decreases and the content of nickel-alumina spinel increases with the increasing calcination temperature, which is due to the formation of the spinel phase at high calcination temperature [37,43]. The above results of Ni species distribution are confirmed from the XRD studies of calcined samples and are also pointed out in the discussion of TPR results. In the previous studies, the NiAl_2O_4 spinel phase was found to be able to enhance the anchoring of the metallic nickel on Al_2O_3 support, which improves the anti-sintering ability of Ni nanoparticles and catalyst thermal stability at high reaction temperatures [37,40,41,52].

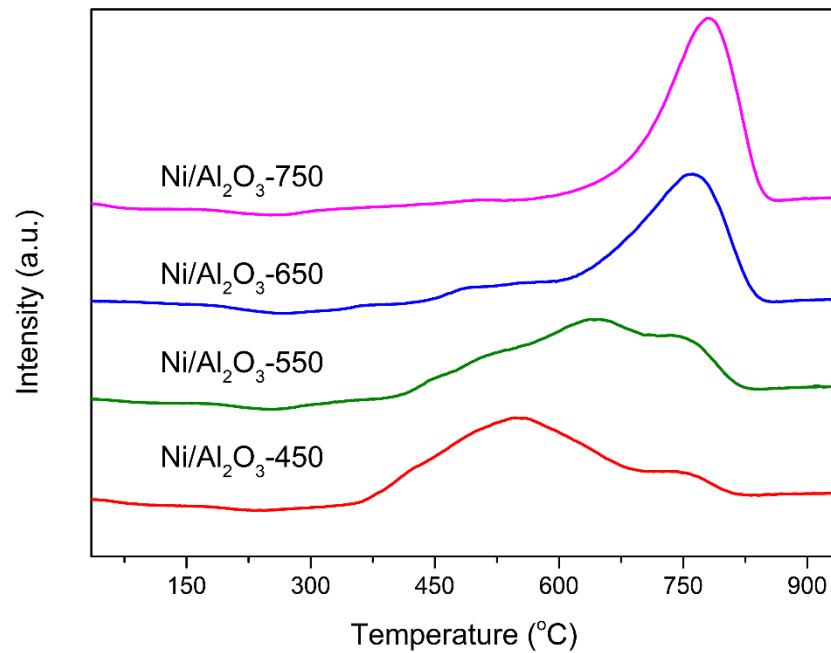


Figure 5. H_2 temperature-programmed reduction (H_2 -TPR) curves of $\text{Ni}/\text{Al}_2\text{O}_3$ samples calcined at different temperatures.

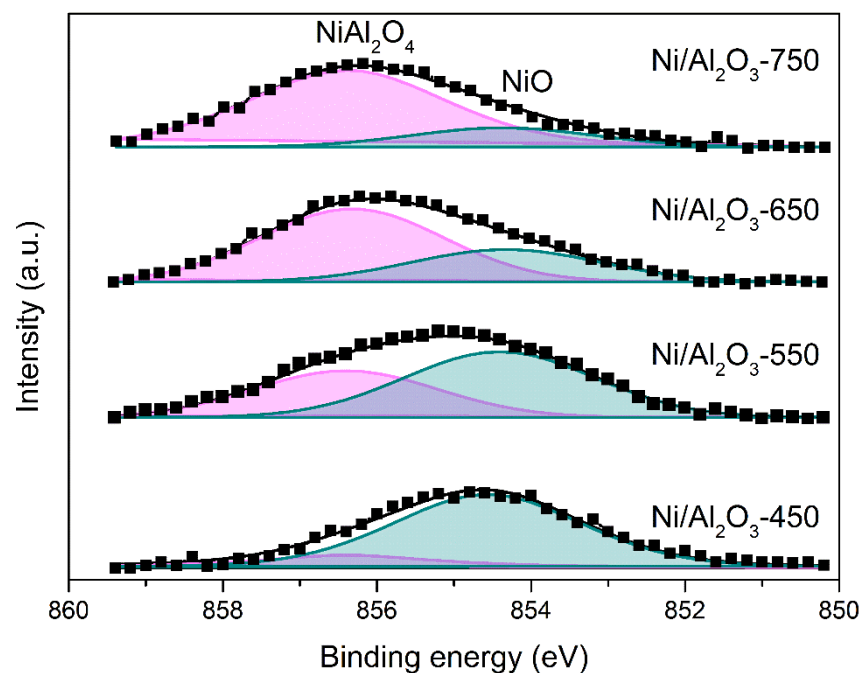


Figure 6. $\text{Ni } 2p_{3/2}$ XPS spectra of $\text{Ni}/\text{Al}_2\text{O}_3$ samples calcined at different temperatures.

3.2. Catalytic Performance for the Dry Reforming of Methane Reaction

3.2.1. Influence of Reaction Temperature on the Activity of the Calcined Catalysts

The catalytic activity of Ni/Al₂O₃ catalysts in the dry reforming of methane reaction was tested in a fixed-bed reactor in the temperature region from 550 to 750 °C under the conditions of 0.1 MPa and GHSV of 24,000 mL g⁻¹ h⁻¹. Figure 7 shows the CH₄ and CO₂ conversion over the four Ni/Al₂O₃ catalysts at different reaction temperatures. The CH₄ and CO₂ conversions monotonically increase as a function of reaction temperature for all the catalysts, these are agreed well with the endothermic nature of the dry reforming of methane reaction (Equation (1)). The CH₄ conversion is lower compared to the CO₂ conversion, which is due to the simultaneous occurrence of a reverse water gas shift reaction (Equation (2)) [10,11,20]. The CH₄ and CO₂ conversions over the catalysts at all reaction temperatures follow the order Ni/Al₂O₃-750 > Ni/Al₂O₃-650 > Ni/Al₂O₃-550 > Ni/Al₂O₃-450, indicating that the CH₄ and CO₂ conversions are strongly dependent on the calcined temperature of the catalysts. The above temperature-dependent performance results reveal that Ni/Al₂O₃ catalysts with small Ni nanoparticles and high Ni dispersion caused by strong metal–support interaction exhibit high catalytic activity. The Ni/Al₂O₃-750 catalyst exhibits the highest catalytic activity at all ranges of temperature, with the CH₄ and CO₂ conversions of 89.8% and 92.9% at 750 °C, respectively. This result is consistent with the small size of the metallic nickel particles present in this catalyst and the high Ni dispersion determined by H₂-TPD analysis (as shown in Table 2).

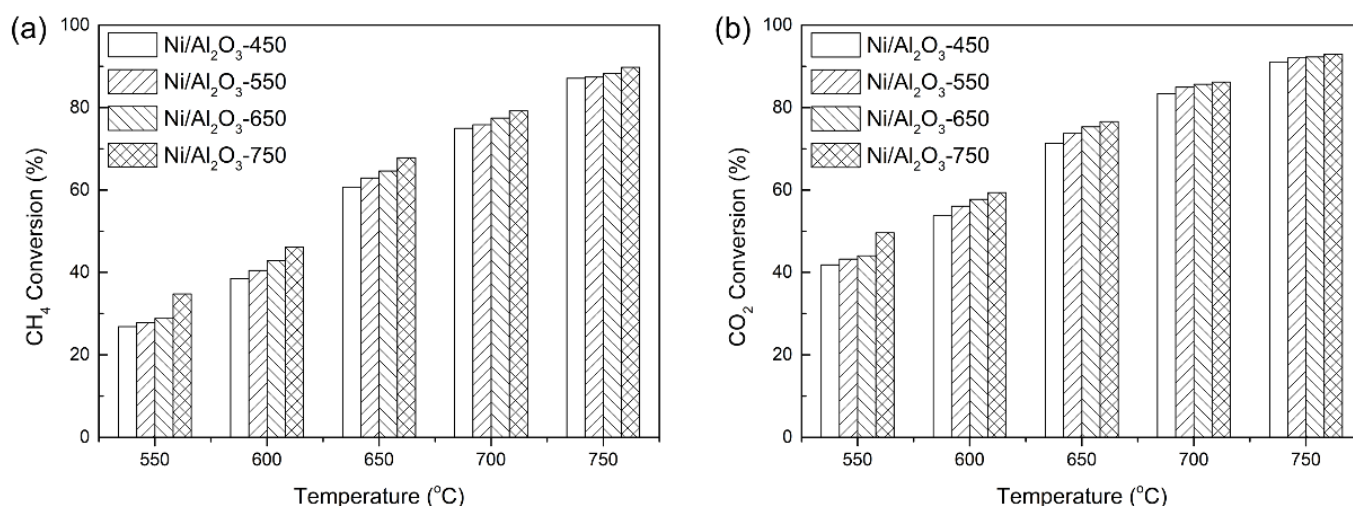


Figure 7. Influence of the reaction temperature on the (a) CH₄ conversions and (b) CO₂ conversions of Ni/Al₂O₃-x catalysts.

3.2.2. Effect of Calcination Temperature on the Catalytic Stability

Preliminary studies of activity performances on Ni/Al₂O₃ catalysts demonstrated that calcination temperature could influence the CH₄ and CO₂ conversions by affecting the Ni nanoparticle size and active component dispersion of the catalysts. Therefore, long-time stability tests were carried out to investigate the performance of the catalysts calcined at different temperatures. The 50 h stability performance of the dry reforming of methane reaction was tested at 700 °C, 0.1 MPa, and GHSV of 24,000 mL g⁻¹ h⁻¹ over all the catalysts. The results in Figure 8 show that the initial catalytic activity increases with increasing calcination temperature, which can be explained based on the difference of Ni dispersion and the Ni⁰ particle size. Ni/Al₂O₃-750 catalyst shows the highest initial CH₄ and CO₂ conversions of 81.0% and 86.5%, respectively. For the stability performance, the Ni/Al₂O₃-750 catalyst displays superior stability among the four catalysts with no obvious deactivation and stable CH₄ and CO₂ conversions during the 50 h reaction. Compared to Ni/Al₂O₃-750, the Ni/Al₂O₃-650 catalyst shows a slight decrease in the initial CH₄ and

CO₂ conversions to 79.6% and 85.3%, respectively, with slight deactivation during 50 h stability test. However, Ni/Al₂O₃-550 and Ni/Al₂O₃-450 catalysts show clear deactivation with the time on stream, and it is more significant over Ni/Al₂O₃-450 catalysts. H₂ and CO yields show similar trends as those for the CH₄ and CO₂ conversions (Figure S2a,b). The results show that the initial H₂ and CO yields increase with the increasing calcination temperature. In addition, the H₂/CO ratios of all four catalysts are lower than 1, which is attributed to the occurrence of reverse water gas shift reaction (Figure S1c). The H₂/CO ratio over Ni/Al₂O₃-750 catalyst remains unchanged in the stability tests. The H₂/CO ratio over the other three catalysts decreases to some extent. The carbon deposition of the Ni/Al₂O₃-x catalysts after 50 h reaction was investigated by TG analysis (Figure S4). It can be seen that the Ni/Al₂O₃-450 catalyst has a large weight loss of ~15%, indicating that a large amount of carbon deposition during the 50 h reaction. However, the spent Ni/Al₂O₃-750 catalyst shows no noticeable weight loss, indicating that the catalyst calcined at high temperature exhibits good performance in coke resistance. The high stability of Ni/Al₂O₃-750 catalyst can be ascribed to the enhanced interaction between the active Ni species and Al₂O₃ support, which leads to small nickel nanoparticles and high Ni dispersion [37,43].

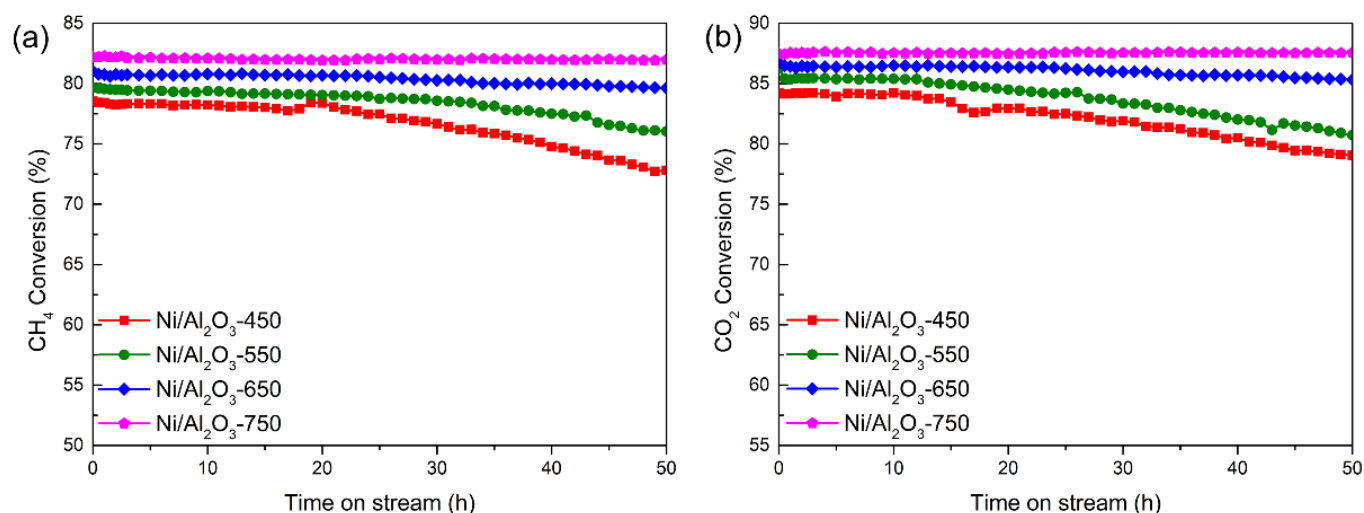


Figure 8. (a) CH₄ conversion and (b) CO₂ conversions as the function of time for stream of Ni/Al₂O₃-x catalysts. Reaction conditions: CH₄:CO₂:Ar = 1:1:3, GHSV = 24,000 mL g⁻¹ h⁻¹, Temperature: 700 °C, atmospheric pressure.

3.2.3. Long-Term Stability Test of the Ni/Al₂O₃-750 Catalyst

It is generally known that the catalysts for dry reforming of methane deactivate rapidly due to the formation of coke that blocks the active metal sites. The coke formation occurs because of the side reactions such as the methane decomposition (Equation (3)) and CO disproportionation reaction (Equation (4)). Therefore, a long-term durability test of 200 h was then carried out at 700 °C to further study the potential application of Ni/Al₂O₃-750 catalyst. In Figure 9, the Ni/Al₂O₃-750 catalyst shows excellent catalytic stability without any noticeable drop during the 200 h reaction. The H₂ yield, CO yield, and H₂/CO ratio of the Ni/Al₂O₃-750 catalyst also remain constant in the long-term stability test (Figure S3). The superior catalytic stability of Ni/Al₂O₃-750 catalyst can be explained from two aspects. On the one hand, the highly dispersed Ni with a small nanoparticle size is prone to expose more active metal sites, which gives rise to the remarkably initial activity. On the other hand, the high dispersion of Ni and the strong metal–support interaction maintain the Ni nanoparticle size during the reaction, which leads to the remarkable stability of Ni/Al₂O₃-750.

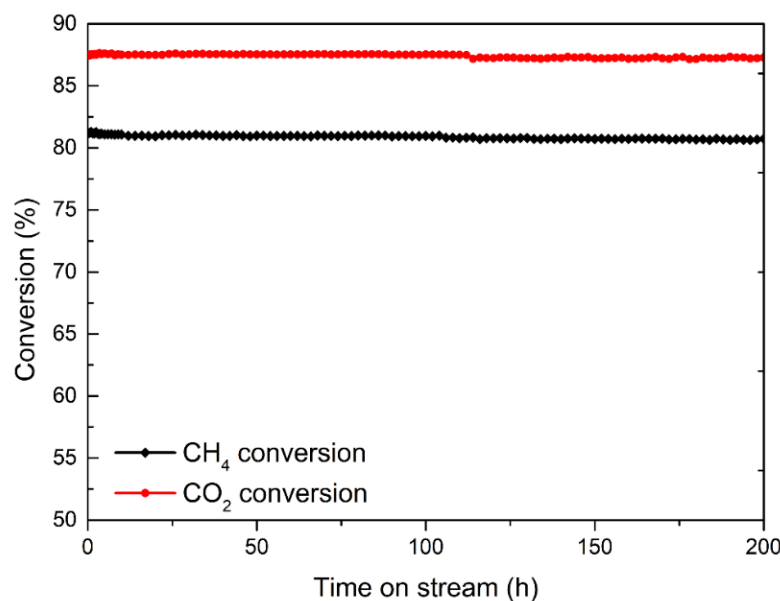


Figure 9. Long-term stability (200 h) test of Ni/Al₂O₃-750 catalyst for dry reforming of methane reaction. Reaction conditions: CH₄:CO₂:Ar = 1:1:3, GHSV = 24,000 mL g⁻¹ h⁻¹, Temperature: 700 °C, atmospheric pressure.

3.3. Characterizations of Spent Ni/Al₂O₃-750 Catalyst after 200 h Dry Reforming of Methane Reaction

Normally, the deactivation of Ni-based catalysts in the dry reforming of methane reaction is caused by the coke formation. Therefore, the spent Ni/Al₂O₃-750 catalyst was characterized in order to study its high catalytic performance.

The crystal structure of the spent Ni/Al₂O₃-750 catalyst was analyzed by XRD (Figure 10). The characteristic peaks of Al₂O₃ indicate that the structure of the spent Ni/Al₂O₃ catalyst remains after the 200 h durability test at the high temperature of 700 °C. The intensity of the peaks assigned to the NiAl₂O₄ spinel greatly decrease, indicating that Ni has been reduced during the pretreatment process in the flow of H₂, which has been proved by the XRD in Figure 3. Ni nanoparticle size (10.1 nm) is estimated from Ni (200) diffraction peak using the Scherrer equation. The small increment of Ni⁰ crystallite size suggests that Ni/Al₂O₃-750 catalyst is resistant to sintering deactivation, attributed to its small Ni nanoparticles, high Ni dispersion, and strong metal–support interaction [45]. On the other hand, the characteristic peak for graphitic carbon (2θ = 26.6°) is not observed in the spent catalyst, implying that there may be less coke formation during the 200 h reaction [33,34].

TG-DTA analysis could provide additional information on deposited carbon on the spent catalysts. Figure 11 presents the TG-DTA curves of the spent Ni/Al₂O₃-750 catalyst. The TG curves can be divided into three parts: the weight loss before 200 °C is ascribed to the removal of adsorbed water, the weight increase at 200–400 °C is due to oxidation of active metallic nickel, and the weight reduction in the region of 400–750 °C is related to the oxidation of deposited carbon. The TG result shows a weight loss of 7.5 wt.% on the spent Ni/Al₂O₃-750, indicating the catalyst has remarkable coke resistance. Normally, based on the DTA curve, the types of deposited carbon are classified into three different carbon species: amorphous carbon species that is easily oxidized (<320 °C), the carbon species between amorphous carbon and graphitic carbon (320–520 °C), and graphitic carbon (>650 °C) [29,32,53,54]. Therefore, it can be reasonably inferred that after 200 h of dry reforming of methane reaction at 700 °C, the carbon species on the Ni/Al₂O₃-750 catalysts are mainly non-graphitic carbon species that can be easily activated and eliminated. Based on the characterization results, it can be explained that the highly stable

Ni nanoparticles with high dispersion obtained at high calcination temperature improve the coking resistance of the Ni/Al₂O₃-750 catalyst.

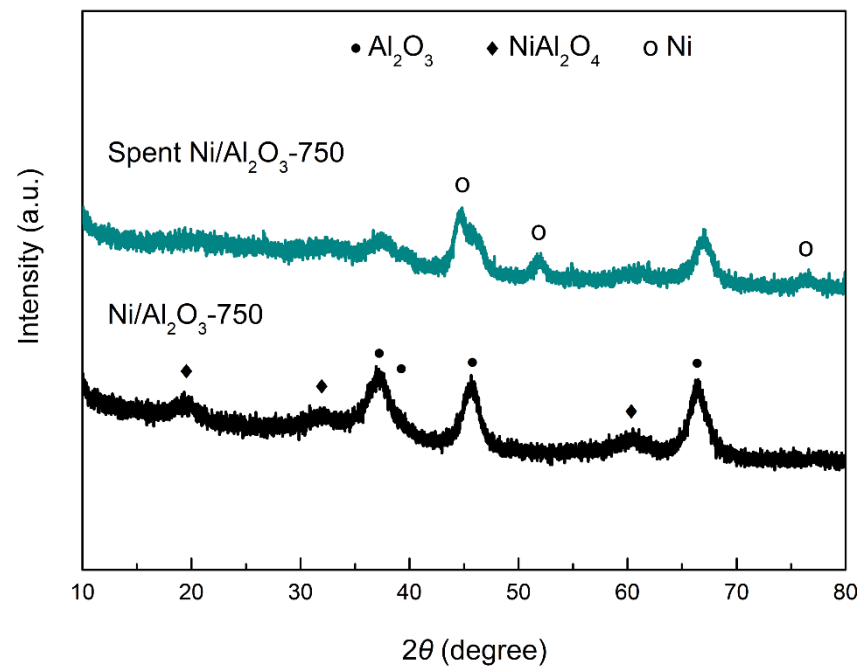


Figure 10. XRD patterns of calcined and spent Ni/Al₂O₃-750 catalysts.

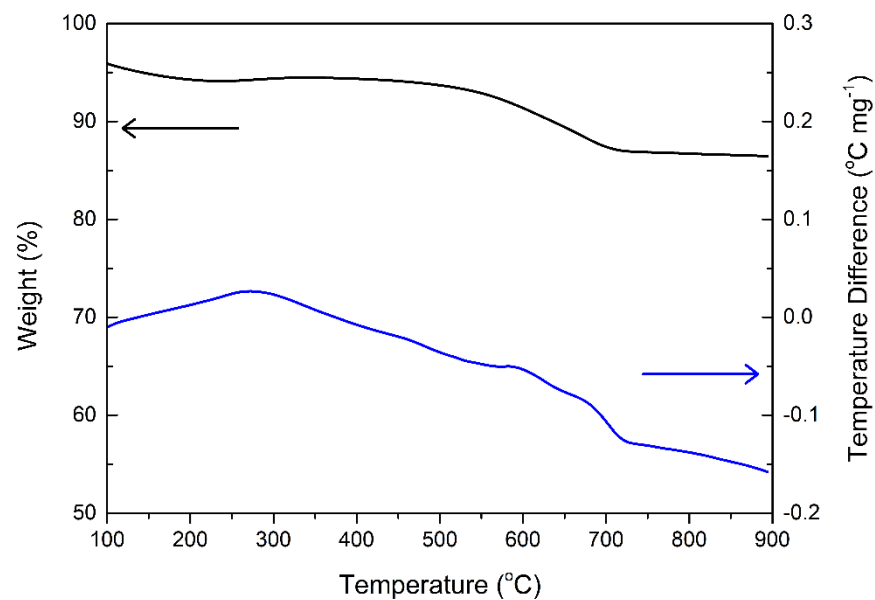


Figure 11. TG-DTA profiles of spent Ni/Al₂O₃-750 catalyst after the 200 h reaction.

According to the previous studies, the calcination temperature had a significant influence on the catalytic performance in the dry reforming of methane reaction [32,40,55–57]. However, the synthesis methods of the catalysts reported in the literature were complicated, and it is desirable to further improve the catalyst stability. In this work, we prepared catalysts by the simple method and enhance the metal–support interaction by increasing calcination temperature, which led to small Ni nanoparticles sizes and high Ni dispersion. Thus, the Ni/Al₂O₃-750 catalyst displayed better catalytic activity and stability compared to the previous studies in the dry reforming of methane reaction.

4. Conclusions

In this work, a series of Ni/Al₂O₃ catalysts with different calcination temperatures (450, 550, 650, and 750 °C) were prepared by the wet impregnation method. The characterization results suggest that calcination temperature significantly affects the surface area, Ni crystallite size, reduction degree, Ni metal dispersion, and metal–support interaction. High calcination temperature leads to the strong interaction between Ni species and alumina to form nickel-alumina spinel. Although increasing the calcination temperature results in a decrease of the surface area and the Ni reduction degree, the effective dispersion increases and the Ni particle size decreases. The catalysts performances show that the activity and stability of Ni/Al₂O₃-x catalysts increase with the increasing calcination temperature. The Ni/Al₂O₃-750 catalyst shows the highest catalytic activity among catalysts studied, along with the superior stability and strong resistance to coke formation after the 200 h stability test at 700 °C.

Supplementary Materials: The following are available online at <https://www.mdpi.com/article/10.3390/pr9040706/s1>, Figure S1: TEM images and Ni particle size distributions of the reduced catalysts: (a) Ni/Al₂O₃-450, (b) Ni/Al₂O₃-550, (c) Ni/Al₂O₃-650, (d) Ni/Al₂O₃-750, Figure S2: (a) H₂ yield, (b) CO yield and (c) H₂/CO ratio as the function of time for stream of Ni/Al₂O₃-x catalysts (50 h test). Reaction conditions: CH₄:CO₂:Ar = 1:1:3, GHSV = 24,000 mL g⁻¹ h⁻¹, 700 °C, atmospheric pressure. Figure S3: H₂ yield, CO yield and H₂/CO ratio of Ni/Al₂O₃-750 catalyst in the long-term stability (200 h) test for dry reforming of methane reaction. Reaction conditions: CH₄:CO₂:Ar = 1:1:3, GHSV = 24,000 mL g⁻¹ h⁻¹, 700 °C, atmospheric pressure. Figure S4: TG analysis of spent Ni/Al₂O₃-x catalysts after the 50 h reaction.

Author Contributions: Methodology, L.H. and B.Y.; Conceptualization, B.Y. and H.H.; Data curation, L.H. and Y.R.; Formal analysis, L.H.; Investigation, L.H.; Project administration, H.H.; Writing—original draft, L.H.; Supervision, H.H. and L.H.; Writing—review and editing, B.Y., S.C.E.T., and H.H. All authors have read and agreed to the published version of the manuscript.

Funding: This research was supported by the National Natural Science Foundation of China (22088101), the Ministry of Science and Technology (2017YFB0602204) and SINOPEC (420068-2).

Conflicts of Interest: The authors declare no conflict of interest.

References

- Zheng, X.S.; Streimikiene, D.; Balezentis, T.; Mardani, A.; Cavallaro, F.; Liao, H. A review of greenhouse gas emission profiles, dynamics, and climate change mitigation efforts across the key climate change players. *J. Clean. Prod.* **2019**, *234*, 1113–1133. [CrossRef]
- Mebrahtu, C.; Krebs, F.; Abate, S.; Perathoner, S.; Centi, G.; Palkovits, R. CO₂ Methanation: Principles and Challenges. In *Horizons in Sustainable Industrial Chemistry and Catalysis*; Elsevier: Amsterdam, The Netherlands, 2019; pp. 85–103. [CrossRef]
- Elvidge, C.D.; Bazilian, M.D.; Zhizhin, M.; Ghosh, T.; Baugh, K.; Hsu, F.C. The potential role of natural gas flaring in meeting greenhouse gas mitigation targets. *Energy Strategy Rev.* **2018**, *20*, 156–162. [CrossRef]
- Yusuf, R.O.; Noor, Z.Z.; Abba, A.H.; Abu Hassan, M.A.; Din, M.F.M. Methane emission by sectors: A comprehensive review of emission sources and mitigation methods. *Renew. Sustain. Energy Rev.* **2012**, *16*, 5059–5070. [CrossRef]
- McFarland, E. Unconventional Chemistry for Unconventional Natural Gas. *Science* **2012**, *338*, 340–342. [CrossRef]
- Aruga, K. The US shale gas revolution and its effect on international gas markets. *J. Unconv. Oil Gas Resour.* **2016**, *14*, 1–5. [CrossRef]
- Banos, R.; Manzano-Agugliaro, F.; Montoya, F.G.; Gil, C.; Alcayde, A.; Gomez, J. Optimization methods applied to renewable and sustainable energy: A review. *Renew. Sustain. Energy Rev.* **2011**, *15*, 1753–1766. [CrossRef]
- Taifan, W.; Baltrusaitis, J. CH₄ conversion to value added products: Potential, limitations and extensions of a single step heterogeneous catalysis. *Appl. Catal. B Environ.* **2016**, *198*, 525–547. [CrossRef]
- Gao, Y.C.; Jiang, J.G.; Meng, Y.; Yan, F.; Aihemaiti, A. A review of recent developments in hydrogen production via biogas dry reforming. *Energy Convers. Manag.* **2018**, *171*, 133–155. [CrossRef]
- Zhao, X.H.; Joseph, B.; Kuhn, J.; Ozcan, S. Biogas Reforming to Syngas: A Review. *iScience* **2020**, *23*, 101082. [CrossRef] [PubMed]
- Li, Z.W.; Lin, Q.; Li, M.; Cao, J.X.; Liu, F.; Pan, H.Y.; Wang, Z.G.; Kawi, S. Recent advances in process and catalyst for CO₂ reforming of methane. *Renew. Sustain. Energy Rev.* **2020**, *134*, 110312. [CrossRef]
- Ellis, P.R.; Enache, D.I.; James, D.W.; Jones, D.S.; Kelly, G.J. A robust and precious metal-free high performance cobalt Fischer-Tropsch catalyst. *Nat. Catal.* **2019**, *2*, 623–631. [CrossRef]

13. Xiong, H.F.; Jewell, L.L.; Coville, N.J. Shaped Carbons as Supports for the Catalytic Conversion of Syngas to Clean Fuels. *ACS Catal.* **2015**, *5*, 2640–2658. [[CrossRef](#)]
14. Galvis, H.M.T.; Bitter, J.H.; Khare, C.B.; Ruitenbeek, M.; Dugulan, A.I.; de Jong, K.P. Supported Iron Nanoparticles as Catalysts for Sustainable Production of Lower Olefins. *Science* **2012**, *335*, 835–838. [[CrossRef](#)] [[PubMed](#)]
15. Zhang, Q.H.; Deng, W.P.; Wang, Y. Recent advances in understanding the key catalyst factors for Fischer-Tropsch synthesis. *J. Energy Chem.* **2013**, *22*, 27–38. [[CrossRef](#)]
16. Zhu, Q.J.; Wegener, S.L.; Xie, C.; Uche, O.; Neurock, M.; Marks, T.J. Sulfur as a selective ‘soft’ oxidant for catalytic methane conversion probed by experiment and theory. *Nat. Chem.* **2013**, *5*, 104–109. [[CrossRef](#)]
17. Tao, X.M.; Bai, M.G.; Li, X.A.; Long, H.L.; Shang, S.Y.; Yin, Y.X.; Dai, X.Y. CH₄-CO₂ reforming by plasma-challenges and opportunities. *Prog. Energy Combust. Sci.* **2011**, *37*, 113–124. [[CrossRef](#)]
18. Zhou, J.; Ye, L.; Huang, D.; Wang, M.; Ren, Y.; Yue, B.; He, H. The synergy of modulated surface polarity and oxygen vacancy for CO₂ to methanol over Zn^(δ-)-Ti^(δ+)O_{vacancy}. *J. Energy Chem.* **2021**, *56*, 449–454. [[CrossRef](#)]
19. Song, Y.; Ozdemir, E.; Ramesh, S.; Adishev, A.; Subramanian, S.; Harale, A.; Albuali, M.; Fadhel, B.A.; Jamal, A.; Moon, D.; et al. Dry reforming of methane by stable Ni-Mo nanocatalysts on single-crystalline MgO. *Science* **2020**, *367*, 777–781. [[CrossRef](#)]
20. Usman, M.; Daud, W.; Abbas, H.F. Dry reforming of methane: Influence of process parameters—A review. *Renew. Sustain. Energy Rev.* **2015**, *45*, 710–744. [[CrossRef](#)]
21. Pakhare, D.; Spivey, J. A review of dry (CO₂) reforming of methane over noble metal catalysts. *Chem. Soc. Rev.* **2014**, *43*, 7813–7837. [[CrossRef](#)]
22. He, L.L.; Ren, Y.H.; Fu, Y.Y.; Yue, B.; Tsang, S.C.E.; He, H.Y. Morphology-dependent catalytic activity of Ru/CeO₂ in dry reforming of methane. *Molecules* **2019**, *24*, 526. [[CrossRef](#)]
23. Singh, S.A.; Madras, G. Sonochemical synthesis of Pt, Ru doped TiO₂ for methane reforming. *Appl. Catal. A Gen.* **2016**, *518*, 102–114. [[CrossRef](#)]
24. Wang, F.G.; Xu, L.L.; Shi, W.D.; Zhang, J.; Wu, K.; Zhao, Y.; Li, H.; Li, H.X.; Xu, G.Q.; Chen, W. Thermally stable Ir/Ce_{0.9}La_{0.1}O₂ catalyst for high temperature methane dry reforming reaction. *Nano Res.* **2017**, *10*, 364–380. [[CrossRef](#)]
25. Batebi, D.; Abedini, R.; Mosayebi, A. Combined steam and CO₂ reforming of methane (CSCRM) over Ni-Pd/Al₂O₃ catalyst for syngas formation. *Int. J. Hydrog. Energy* **2020**, *45*, 14293–14310. [[CrossRef](#)]
26. Jiang, C.; Loisel, E.; Cullen, D.A.; Dorman, J.A.; Dooley, K.M. On the enhanced sulfur and coking tolerance of Ni-Co-rare earth oxide catalysts for the dry reforming of methane. *J. Catal.* **2021**, *393*, 215–229. [[CrossRef](#)]
27. Kim, W.Y.; Lee, Y.H.; Park, H.; Choi, Y.H.; Lee, M.H.; Lee, J.S. Coke tolerance of Ni/Al₂O₃ nanosheet catalyst for dry reforming of methane. *Catal. Sci. Technol.* **2016**, *6*, 2060–2064. [[CrossRef](#)]
28. Zhang, J.; Li, F. Coke-resistant Ni@SiO₂ catalyst for dry reforming of methane. *Appl. Catal. B Environ.* **2015**, *176*, 513–521. [[CrossRef](#)]
29. Cai, W.; Ye, L.; Zhang, L.; Ren, Y.; Yue, B.; Chen, X.; He, H. Highly Dispersed Nickel-Containing Mesoporous Silica with Superior Stability in Carbon Dioxide Reforming of Methane: The Effect of Anchoring. *Materials* **2014**, *7*, 2340–2355. [[CrossRef](#)]
30. Morales-Marin, A.; Ayastuy, J.L.; Iriarte-Velasco, U.; Gutierrez-Ortiz, M.A.; Chemical Technologies, E. Nickel aluminate spinel-derived catalysts for the aqueous phase reforming of glycerol: Effect of reduction temperature. *Appl. Catal. B Environ.* **2019**, *244*, 931–945. [[CrossRef](#)]
31. Kim, H.M.; Kim, B.J.; Jang, W.J.; Shim, J.O.; Jeon, K.W.; Na, H.S.; Lee, Y.L.; Jeon, B.H.; Roh, H.S. Effect of support materials and Ni loading on catalytic performance for carbon dioxide reforming of coke oven gas. *Int. J. Hydrog. Energy* **2019**, *44*, 8233–8242. [[CrossRef](#)]
32. Al-Fatesh, A.S.; Abu-Dahrieh, J.K.; Atia, H.; Armbruster, U.; Ibrahim, A.A.; Khan, W.U.; Abasaed, A.E.; Fakeeha, A.H. Effect of pre-treatment and calcination temperature on Al₂O₃-ZrO₂ supported Ni-Co catalysts for dry reforming of methane. *Int. J. Hydrog. Energy* **2019**, *44*, 21546–21558. [[CrossRef](#)]
33. Das, S.; Ashok, J.; Bian, Z.; Dewangan, N.; Wai, M.H.; Du, Y.; Borgna, A.; Hidajat, K.; Kawi, S. Silica-Ceria sandwiched Ni core-shell catalyst for low temperature dry reforming of biogas: Coke resistance and mechanistic insights. *Appl. Catal. B Environ.* **2018**, *230*, 220–236. [[CrossRef](#)]
34. Li, J.; Ren, Y.H.; Yue, B.; He, H.Y. Ni/Al₂O₃ catalysts derived from spinel NiAl₂O₄ for low-temperature hydrogenation of maleic anhydride to succinic anhydride. *Chin. J. Catal.* **2017**, *38*, 1166–1173. [[CrossRef](#)]
35. Giehr, A.; Maier, L.; Schunk, S.A.; Deutschmann, O. Thermodynamic Considerations on the Oxidation State of Co/γ-Al₂O₃ and Ni/γ-Al₂O₃ Catalysts under Dry and Steam Reforming Conditions. *ChemCatChem* **2018**, *10*, 751–757. [[CrossRef](#)]
36. Kumar, R.; Kumar, K.; Choudary, N.V.; Pant, K.K. Effect of support materials on the performance of Ni-based catalysts in tri-reforming of methane. *Fuel Process. Technol.* **2019**, *186*, 40–52. [[CrossRef](#)]
37. Smolakova, L.; Kout, M.; Koudelkova, E.; Capek, L. Effect of Calcination Temperature on the Structure and Catalytic Performance of the Ni/Al₂O₃ and Ni-Ce/Al₂O₃ Catalysts in Oxidative Dehydrogenation of Ethane. *Ind. Eng. Chem. Res.* **2015**, *54*, 12730–12740. [[CrossRef](#)]
38. Jeon, K.W.; Shim, J.O.; Jang, W.J.; Lee, D.W.; Na, H.S.; Kim, H.M.; Lee, Y.L.; Yoo, S.Y.; Roh, H.S.; Jeon, B.H.; et al. Effect of calcination temperature on the association between free NiO species and catalytic activity of Ni-Ce_{0.6}Zr_{0.4}O₂ deoxygenation catalysts for biodiesel production. *Renew. Energy* **2019**, *131*, 144–151. [[CrossRef](#)]

39. Katheria, S.; Gupta, A.; Deo, G.; Kunzru, D. Effect of calcination temperature on stability and activity of Ni/MgAl₂O₄ catalyst for steam reforming of methane at high pressure condition. *Int. J. Hydrog. Energy* **2016**, *41*, 14123–14132. [[CrossRef](#)]
40. Smolakova, L.; Kout, M.; Capek, L.; Rodriguez-Gomez, A.; Gonzalez-Delacruz, V.M.; Hromadko, L.; Caballero, A. Nickel catalyst with outstanding activity in the DRM reaction prepared by high temperature calcination treatment. *Int. J. Hydrog. Energy* **2016**, *41*, 8459–8469. [[CrossRef](#)]
41. Al-Fatesh, A.S.A.; Fakeeha, A.H. Effects of calcination and activation temperature on dry reforming catalysts. *J. Saudi Chem. Soc.* **2012**, *16*, 55–61. [[CrossRef](#)]
42. Zhang, C.; Hu, X.; Zhang, Z.; Zhang, L.; Dong, D.; Gao, G.; Westerhof, R.; Syed-Hassan, S.S.A. Steam reforming of acetic acid over Ni/Al₂O₃ catalyst: Correlation of calcination temperature with the interaction of nickel and alumina. *Fuel* **2018**, *227*, 307–324. [[CrossRef](#)]
43. Wang, Y.; Liang, D.; Wang, C.; Chen, M.; Tang, Z.; Hu, J.; Yang, Z.; Zhang, H.; Wang, J.; Liu, S. Influence of calcination temperature of Ni/Attapulgite on hydrogen production by steam reforming ethanol. *Renew. Energy* **2020**, *160*, 597–611. [[CrossRef](#)]
44. Zhao, A.M.; Ying, W.Y.; Zhang, H.T.; Ma, H.F.; Fang, D.Y. Ni-Al₂O₃ catalysts prepared by solution combustion method for syngas methanation. *Catal. Commun.* **2012**, *17*, 34–38. [[CrossRef](#)]
45. Wei, Q.; Gao, X.; Wang, L.; Ma, Q. Rational design of nickel-based catalyst coupling with combined methane reforming to steadily produce syngas. *Fuel* **2020**, *271*, 117631. [[CrossRef](#)]
46. Jimenez-Gonzalez, C.; Boukha, Z.; de Rivas, B.; Delgado, J.J.; Cauqui, M.A.; Gonzalez-Velasco, J.R.; Gutierrez-Ortiz, J.I.; Lopez-Fonseca, R. Structural characterisation of Ni/alumina reforming catalysts activated at high temperatures. *Appl. Catal. A Gen.* **2013**, *466*, 9–20. [[CrossRef](#)]
47. Lee, Y.-L.; Kim, B.-J.; Park, H.-R.; Ahn, S.-Y.; Kim, K.-J.; Roh, H.-S. Customized Ni-MgO-Al₂O₃ catalyst for carbon dioxide reforming of coke oven gas: Optimization of preparation method and co-precipitation pH. *J. CO₂ Util.* **2020**, *42*, 101354. [[CrossRef](#)]
48. Parastaev, A.; Muravev, V.; Osta, E.H.; van Hoof, A.J.F.; Kimpel, T.F.; Kosinov, N.; Hensen, E.J.M. Boosting CO₂ hydrogenation via size-dependent metal-support interactions in cobalt/ceria-based catalysts. *Nat. Catal.* **2020**, *3*, 526–533. [[CrossRef](#)]
49. Li, C.P.; Proctor, A.; Hercules, D.M. Curve fitting analysis of ESCA Ni 2p spectra of Nickel-Oxygen compounds and Ni/Al₂O₃ catalysts. *Appl. Spectrosc.* **1984**, *38*, 880–886. [[CrossRef](#)]
50. Huang, T.T.; Peng, Q.Y.; Shi, W.J.; Xu, J.D.; Fan, Y. An anionic surfactant-assisted equilibrium adsorption method to prepare highly dispersed Fe-promoted Ni/Al₂O₃ catalysts for highly selective mercaptan removal. *Appl. Catal. B Environ.* **2018**, *230*, 154–164. [[CrossRef](#)]
51. Mansour, A.N. Characterization of NiO by XPS. *Surf. Sci. Spectra* **1994**, *3*, 231–238. [[CrossRef](#)]
52. Zhang, Z.M.; Hu, X.; Li, J.J.; Gao, G.G.; Dong, D.H.; Westerhof, R.; Hu, S.; Xiang, J.; Wang, Y. Steam reforming of acetic acid over Ni/Al₂O₃ catalysts: Correlation of nickel loading with properties and catalytic behaviors of the catalysts. *Fuel* **2018**, *217*, 389–403. [[CrossRef](#)]
53. Cao, K.; Gong, M.; Yang, J.F.; Cai, J.M.; Chu, S.Q.; Chen, Z.P.; Shan, B.; Chen, R. Nickel catalyst with atomically-thin meshed cobalt coating for improved durability in dry reforming of methane. *J. Catal.* **2019**, *373*, 351–360. [[CrossRef](#)]
54. Zhang, Q.L.; Sun, M.H.; Ning, P.; Long, K.X.; Wang, J.; Tang, T.; Fan, J.; Sun, H.Y.; Yin, L.T.; Lin, Q. Effect of thermal induction temperature on re-dispersion behavior of Ni nanoparticles over Ni/SBA-15 for dry reforming of methane. *Appl. Surf. Sci.* **2019**, *469*, 368–377. [[CrossRef](#)]
55. Katheria, S.; Deo, G.; Kunzru, D. Rh-Ni/MgAl₂O₄ catalyst for steam reforming of methane: Effect of Rh doping, calcination temperature and its application on metal monoliths. *Appl. Catal. A Gen.* **2019**, *570*, 308–318. [[CrossRef](#)]
56. Bian, Z.; Zhong, W.; Yu, Y.; Wang, Z.; Jiang, B.; Kawi, S. Dry reforming of methane on Ni/mesoporous-Al₂O₃ catalysts: Effect of calcination temperature. *Int. J. Hydrog. Energy* **2021**. [[CrossRef](#)]
57. Xu, Y.; Du, X.; Shi, L.; Chen, T.; Wan, H.; Wang, P.; Wei, S.; Yao, B.; Zhu, J.; Song, M. Improved performance of Ni/Al₂O₃ catalyst deriving from the hydrotalcite precursor synthesized on Al₂O₃ support for dry reforming of methane. *Int. J. Hydrog. Energy* **2021**, *46*, 14301–14310. [[CrossRef](#)]